Catena 182 (2019) 104118

Contents lists available at ScienceDirect

Catena

journal homepage: www.elsevier.com/locate/catena

Exploring extreme rainfall impacts on flow and turbidity dynamics in a steep, pristine and tropical volcanic catchment

Vanessa Solano-Rivera[a], Josie Geris[b], Sebastián Granados-Bolaños[a], Liz Brenes-Cambronero[c], Guillermo Artavia-Rodríguez[a], Ricardo Sánchez-Murillo[d], Christian Birkel[a,b,*]

[a] Department of Geography and Water and Global Change Observatory, University of Costa Rica, 2060 San José, Costa Rica
[b] Northern Rivers Institute, University of Aberdeen, AB24 3UF Aberdeen, United Kingdom of Great Britain and Northern Ireland
[c] ReBAMB, Sede de Occidente, University of Costa Rica, 2060 San José, Costa Rica
[d] Stable Isotope Research Group, National University of Costa Rica, Heredia, Costa Rica

ARTICLE INFO

Keywords:
Tropics
Costa Rica
Turbidity
Erosion
Volcanic and fluvial geomorphology
Extreme rainfall events, ReBAMB

ABSTRACT

Tropical volcanic landscapes are important because of the short timescales (< years) over which they transform. Sediment sources, availability and transport can be highly dynamic, but our understanding of these is limited by a lack of data in these complex environments, especially with regards to extreme events. To investigate the responses to extreme rainfall events in particular, we conducted extensive monitoring in a pristine tropical rainforest catchment (3.2 km^2), located in the Volcanic Cordillera of Tilarán, Costa Rica. We established high temporal resolution hydro-meteorological and turbidity monitoring from June 2015 to July 2016. This included a record convective rainfall event in August 2015 which resulted in an estimated > 50 yr return period flood event. We also surveyed hillslope soils, landslides, and sediments of the river network, to characterize sediments before and after the extreme event. Our results suggested that rainfall events activated surface flow pathways with associated mobilization of material. However, erosion processes were mostly linked to finer material (sand, silt) properties of the soils that developed on more highly weathered bedrock. The single extreme event (return period > 50 years) had an overriding impact on the general sediment dynamics. Recovery in the form of fine material transport and associated hysteresis took only about three months. We conclude that the combined use of high-temporal resolution monitoring with spatially distributed surveys provided new insights for the initial assessment into the fluvial geomorphology and transport dynamics of steep, volcanic headwater catchments in the humid tropics with potential to establish more complete time scales of land-forming processes. This work can build the foundation for more complete monitoring using radioisotopes as a tool to fingerprint the sediment origin and composition.

1. Introduction

Tropical ecosystems experience an accelerated land use change (Foley et al., 2005) and are climate change hot spots, particularly in Central America (Giorgi, 2006; González et al., 2017). Despite the deforestation ban in Costa Rica which increased the national forest cover over the last 30 years (Fagan et al., 2013), there is a prevalent trend towards deforestation in the wider region. The associated impacts of these changes on hydrological processes and sediment dynamics in the tropics have received much interest (Chappell et al., 2004; Bonell and Bruijnzeel, 2005). An increasing number of studies have examined sediment dynamics across a wide range of catchments (Fryers, 2013; Buendia et al., 2015). However, these studies have focussed mostly on anthropogenically-impacted catchments (e.g. agriculture), where human disturbance accelerates the natural process of erosion-transport-deposition (Walsh et al., 2011). Research conducted in undisturbed forested areas is limited (see Zhang et al., 2010 as an exception and a global review by Zimmermann et al., 2012), particularly in tropical forests with a geomorphology of volcanic origin (see Muñoz-Villers and McDonnell, 2012, for an example with emphasis on rainfall-runoff dynamics) where the natural dynamics of erosion and deposition processes are mostly unknown.

Abbreviations: AWI7d, antecedent wetness 7 days (mm); M, precipitation magnitude (mm); Imax, maximum intensity (mm/h); P_Qlag, lag between the peaks of precipitation and discharge (h); Range, turbidity range from beginning to the event peak (NTU); P_NTUlag, lag between the peaks of precipitation and turbidity (h); NTU_Qlag, lag between the peaks of discharge and turbidity (h); Qrange, discharge range from beginning to the event peak (m^3/s)

* Corresponding author at: Department of Geography and Water and Global Change Observatory, University of Costa Rica, 2060 San José, Costa Rica.
E-mail address: christian.birkel@ucr.ac.cr (C. Birkel).

https://doi.org/10.1016/j.catena.2019.104118
Received 29 October 2018; Received in revised form 23 April 2019; Accepted 10 June 2019

Furthermore, the tropics are generally characterized by high rainfall rates (Chang and Lau, 1983), which - even under undisturbed vegetation cover - can result in surface flow, erosion and subsequently naturally high sediment loads (Thomas, 1994). In such catchments, the erosion-transport-deposition dynamics tend to be flashy and variable due to the heterogeneity of the climate and the material properties of the soils and bedrock. The soil characteristics with e.g. low hydraulic conductivity, as observed in a lowland rainforest catchment in Panamá, importantly influence the runoff generation processes with surface flow as the most prominent erosion mechanism (Zimmermann et al., 2012).

Headwater systems globally amount to almost 80% of delivered water and transported substances to rivers (Downing et al., 2012), but remain largely unmonitored. Within the tropics, volcanic landscapes are of specific interest because of the short timescales (< years) over which they transform (Wohl et al., 2012). This may cause severe consequences for downstream water users (e.g. hydropower, drinking water, irrigation, and other ecosystem services). Understanding the formation and evolution of volcanic landscapes in the tropics therefore involves an analysis of the effects of intense and prolonged rainfall events on sediment dynamics and hydrological processes at the event scale. Sediment mobilization can be (initiated) via:

a) shallow landslides and debris flows due to the saturation of the soils contributing material to the streams,
b) laminar erosion on the hillslopes connected to the stream due to surface runoff even under pristine forest cover and.
c) the transport dynamics and erosion of the stream, banks and streambed itself.

However, a major challenge in both geomorphology and hydrology is reconciling the disparity between small scale measurements with larger spatial and temporal scale processes (Bracken et al., 2013). One way to assess the integrated response of the system at catchment scales is by linking spatially distributed point scale measurements to high temporal resolution measurements in the stream (Hancock and Lowry, 2015). Alternative approaches include measurements in nested catchments such as by López-Tarazón and Estrany (2017) in the Mediterranean untangling the drivers of sediment transport and their temporal characteristics. Similarly, Mills and Bathurst (2015) successfully developed a predictive suspended sediment load relationship with spatially distributed catchment characteristics and sediment sources in the UK. However, long-term catchment studies in the tropics are rare (see exceptions from Puerto Rico reported by Shanley et al., 2011 and Thailand by Ziegler et al., 2014), despite that small-scale and detailed measurements may lead to insights into the longer-term landscape forming processes of steep, tropical volcanic catchments and the role extreme events might play.

In Costa Rica, Krishnaswamy et al. (2001a) found that suspended sediment transport was linked to climate dynamics and land use disturbances in a large (~5000 km^2) heterogeneous catchment. In addition, Calvo (1998) attempted to model suspended sediment yields for various larger catchments and found that rainfall erosivity and land use were important drivers of sediment transport. Jansson (2002) explored sediment origin using hysteresis analysis in a meso-scale catchment draining the Caribbean in central Costa Rica. However, these studies followed a relatively coarse temporal resolution (roughly monthly and few events in the case of Jansson, 2002) sampling of suspended sediments, so that the highly dynamic nature of processes during events could not be captured. Following previous larger-scale efforts (e.g. Krishnaswamy et al., 2001b), here, via intense monitoring, we aimed to gain more insights into the sediment transport dynamics in humid tropical volcanic landscapes, with a specific focus on exploring responses to extreme rainfall events. The monitoring included high temporal resolution turbidity, hillslope soil erosion, material properties of soil and sediments, and hydrometric data collected over one hydrological year in the San Lorencito catchment (a 3.2 km^2 tropical pristine headwater catchment) in the Volcanic Cordillera of Tilarán, Costa Rica. Using field and laboratory data and statistical analyses, this study is one of the first in humid tropical volcanic environments that explores when, how and where sediment transport is generated associated with hydrological processes and catchment responses to intense rainfall events, within the possibilities of a complex and logistically challenging field site. We also tested the utility of turbidity as an indicator of suspended sediment loads in a highly dynamic, volcanic catchment for a relatively short measurement period. The specific objectives were to:

(i) monitor and analyse the stream response and subsequent turbidity dynamics to rainfall inputs at high temporal resolution,
(ii) characterize the impact of an extreme event on the rainfall-runoff-turbidity and sediment relationship, fluvial geomorphology, and the subsequent recovery of the system,
(iii) explore how in-stream dynamics are linked to hillslope sediment sources, their connectivity to the stream, and potential changes to sediment sources induced by extreme events.

2. Study area and methods

2.1. Catchment characteristics

The humid tropical San Lorencito headwater catchment drains an area of 3.2 km^2 towards the Caribbean Sea in the northern mountainous area of Costa Rica known as Cordillera de Tilarán (Fig. 1). The catchment is located in the Biological Reserve Alberto Manuel Brenes (ReBAMB), a protected area with restricted access only for research. Land cover involves a typical primary montane rainforest with negligible human intervention (Fig. 1e). The most prominent tree species are *Elaegiaux panamensis* and *Ocotea morae*, palmito (*Iriartea deltoidea)* and various types of higuerones (*Ficus spp*.) (Salazar-Rodríguez, 2003).

The geology is composed of tertiary volcanic rocks (5–9 million years), mainly from extrusive materials such as basalts, andesites, and pyroclastic flow deposits typical of violent volcanic activity during the younger Miocene Epoch (Bergoeing, 2007) from a nearby emission source in the upper extreme of the catchment (Fig. 1b). The morphology of the catchment is characterized by steep slopes (> 30%). The high annual rainfall is around 3 m/yr with around 2 m/yr of discharge (Table I). The main stream follows a normal fault line (Fig. 1b) resulting in two slightly different main hillslopes. The northern or left hillslope (B, upstream view) shows on average more basalt and more andesitic mineralogy than on the southern or right hillslope (A, Fig. 2). Hillslope A is also on average less steep and deeper soils developed compared to those on hillslope B. The soils originating from hillslope A were characterized by loamy and sandy loam particle size, while the soils from hillslope B had less sandy particles and showed some presence of clay (< 30%). Soil characteristics are related to the volcanic geomorphology of the catchment with less developed, coarse textured Entisols or alluvial soil profiles near the stream. Closer to the hilltops deeper Andisols (> 1 m) with higher organic matter content (> 20%) and almost permanent saturation can be found. Remnants of volcanic ash in the upper profiles are common (0–0.5 m). More information on catchment characteristics and the hydrology of the study site can be found in Dehaspe et al. (2018).

The climate is characterized by a constantly high humidity close to 100% throughout the year with a prolonged rainy season during the months from May to December and a short dry season from January to April. Nevertheless, rain events are common throughout the year (Fig. 1d). The study area is situated at the continental divide and is predominantly under the influence of north-eastern trade winds that are responsible for the influx of humidity. The latter in combination with local, intense convective rainstorms generate very high rainfall rates well exceeding 40 mm/h leading to a rapid stream response. Deviations from normal weather patterns are introduced by frontal systems from the northern hemisphere winter, indirect effects of

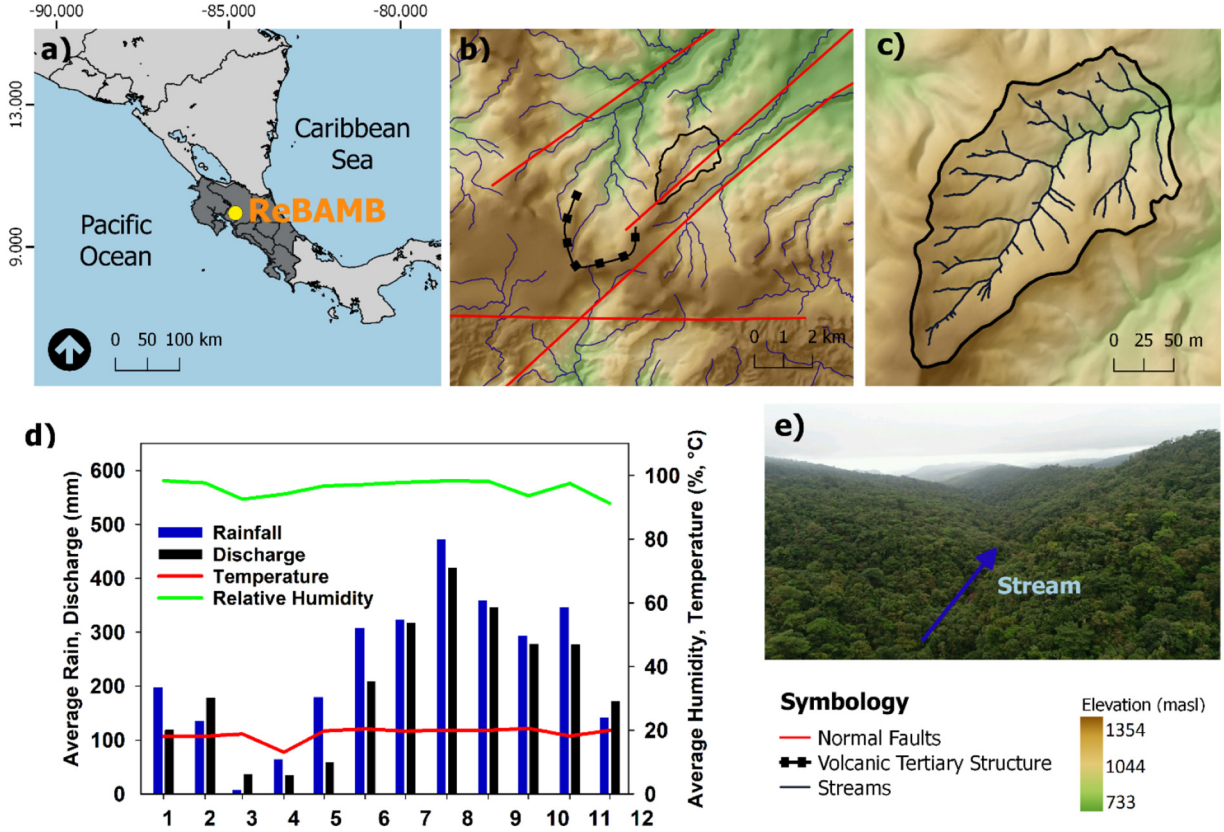

Fig. 1. a) Regional context showing the location of the San Lorencito catchment in Costa Rica, Central America with b-c) topography, volcanic, and tectonic geological features (fault lines and the tertiary volcano remnant) that affect sediment dynamics (Denyer et al., 2003), d) monthly climate regime from January to December (1 to 12) based on the measurements of 2015–2016, and e) aerial image of the dense rainforest.

Table I
Basic catchment descriptors and data properties for hydro-meteorological and geomorphologic context.

Descriptor	Unit	Mean [range]
Area	km^2	3.2
Topography		
Elevation	m.a.s.l.	1133.5 [873.7–1472.4]
Slope	°	22.3 [0.15–52]
Drainage density (1:200000)	km/km^2	0.016
Stream slope	°	20.5
Sediment transport index		17.04 [0–390]
Terrain ruggedness index		1.63 [0.01–5.03]
Hydroclimatic		
Annual P 2015–2016	mm	2762
Annual PET 2015–2016	mm	425
Annual Q 2015–2016	mm	2448

hurricanes and the El Niño Southern Oscillation (ENSO) resulting in either increased or less rainfall (Birkel et al., 2016).

The San Lorencito stream is highly dynamic and bed materials are generally composed of volcanic angular and sub-angular boulders disposed in large banks along the riverbed. The fluvial geomorphology is dominated by step-pool features with some cascades (Fig. 2A and C) and characterized by the occurrence of frequent landslides (Fig. 2G) that deposit materials along fluvial terraces (Fig. 2F). Stream morphology is also affected by erosion that removes material from the banks and riverbed. Minor alluvial fans can be found along the stream tributaries with available large boulders and sediments to be transported in extreme conditions (Fig. 2E).

2.2. Field measurements and laboratory analysis

In-situ sensors measured turbidity (Global Water WQ730, NTU) and water level (Global Water WL400–015-025) in an accessible and relatively protected section at the outlet of the San Lorencito catchment over one year from June 2015 to July 2016. Sensors were placed within a 30 kg steel cage and PVC tubes for protection and routinely cleaned and calibrated. Data were stored every 5 min using a Global Water GL-500 logger. Meteorological data (rainfall, temperature, humidity, radiation, pressure, wind direction and speed) were measured using a Davis Vantage Pro Plus 2 station (MS1) programmed to 30-min time steps in a cleared spot located 1 km NE outside the study catchment (Fig. 3). It is well known that both sloping ground (e.g. Sharon, 1980) and canopy interception (e.g. Loescher et al., 2002) can introduce complexity and variability in the observations of rainfall. To assess the extent to which the complete but single rainfall records of the meteorological station could be used for this study, we therefore initially explored the effects of spatial variability and altitudinal gradients (total elevation gradient is 460 m). For this, throughfall measurements (HOBO rain gauges) were taken at different times during the rainy season from June to December 2015 at two locations: one close to the stream (at 890 m a.s.l) and on the left hilltop at 1232 m a.s.l (Fig. 2 – MS2 and MS3, respectively). We found that throughfall at MS2 and MS3 and gross precipitation measured at the meteorological station followed identical event timings in terms of peak rainfall with slight differences in measured volumes (< 10%) due to the intercepting vegetation. No significant precipitation elevation gradient was detected over the relatively short distance that concerns the study site and we do not show this preliminary analysis here. Therefore, we used the continuous measurements of gross rainfall at the meteorological station for further event analysis.

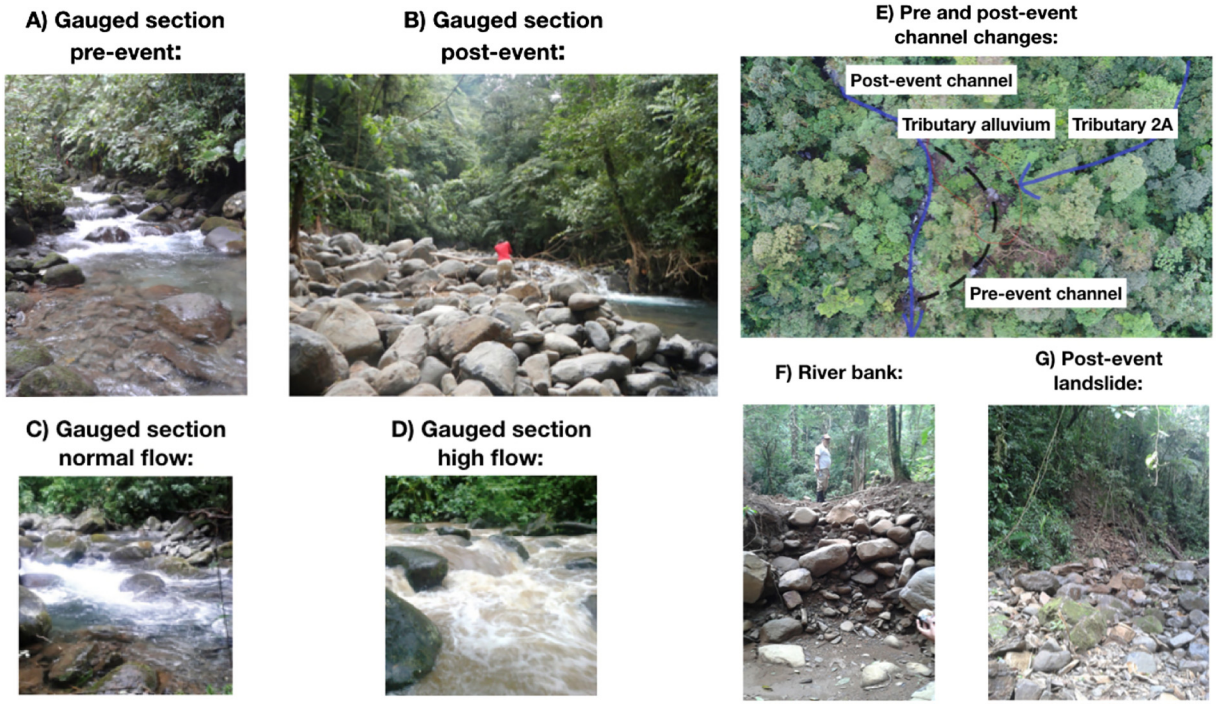

Fig. 2. A and B) The pre-event step-pool stream morphology looking upstream from the gauged section and the widened post-event section with material deposits. C and D) show the flow in normal conditions and high flow with turbid water. E) Reconstructed stream channel modifications and the tributary influence in contributing alluvial material. F) Post-event eroded stream bank showing the previously deposited fluvial material. G) Post-event landslide incorporating fresh material into the stream.

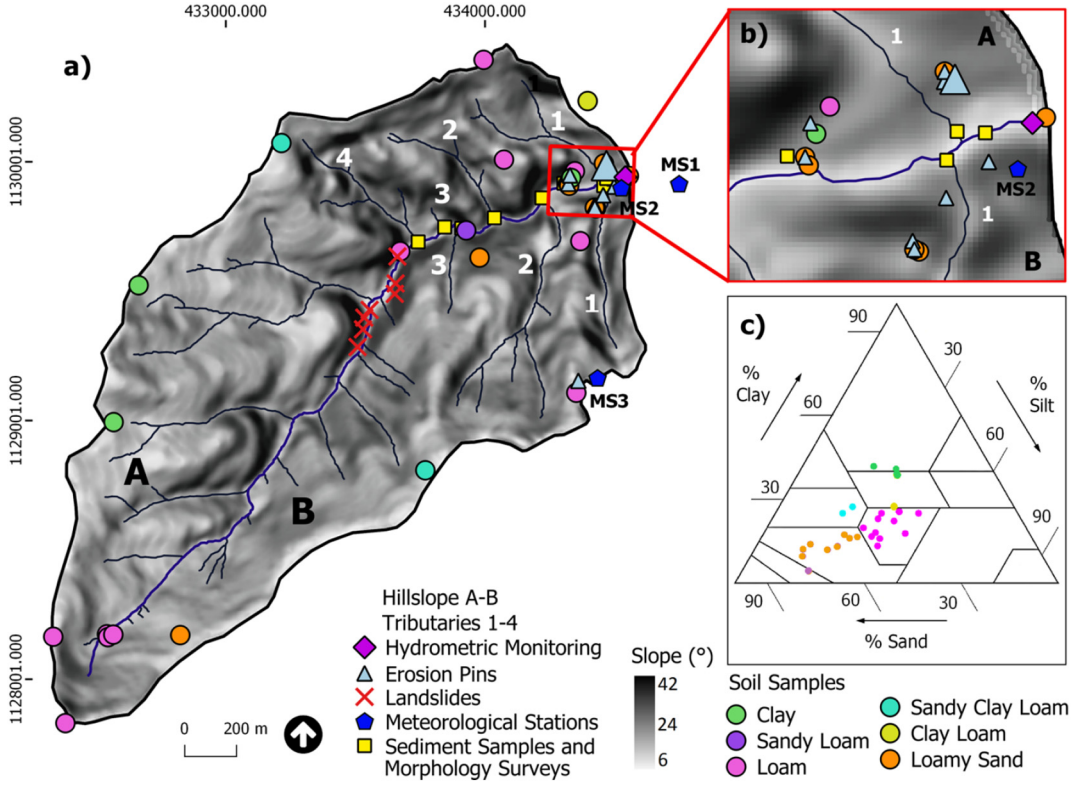

Fig. 3. a) The slope map (grey scale) shows the location of monitoring equipment (hydrometric and meteorological stations MS with MS1 recording gross precipitation and MS2 and MS3 throughfall) and spatial surveys, b) the detailed map indicates the locations of soil, erosion (larger triangle shows the largest soil erosion measurement), landslides and sediment surveys dictated by site access, and c) the distribution of the processed and colour coded soil samples across the United States Department of Agriculture (USDA) texture triangle.

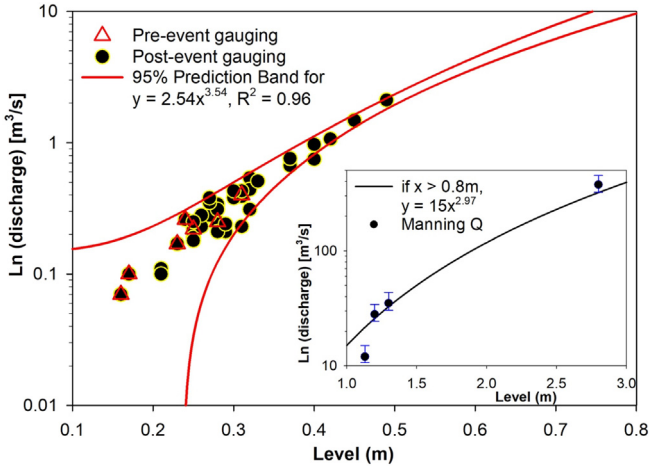

Fig. 4. The preliminary two-stage rating curve for the San Lorencito stream based on 37 manual gaugings (7 pre-event in red triangles and 30 post-event in yellow-black circles) and four re-constructed largest peak flows with overbank flow using Manning's equation (inlet graph). The error bars were calculated systematically varying Manning's n roughness coefficient. (For interpretation of the references to colour in this figure legend, the reader is referred to the web version of this article.)

Throughout the entire monitoring period, manual discharge gaugings (salt dilution and current meter) were done approximately every 3 weeks and on an occasional event-basis. The difference between both measurement techniques was below 10% of absolute gauged streamflows. These gaugings were used in the construction of a rating curve that converts measured water level into discharge (m^3/s) (Fig. 4). During very high flows (at levels > 0.8 m), overbank flow occurred. We therefore applied a separate rating curve for these higher levels by applying Manning's equation to events with recorded flood marks (four in total). We tested the sensitivity of the resulting discharge estimate by varying the Manning coefficient n for mountain streams with cobbles and large boulders in between a range of 0.04 to 0.07 (Chow, 1959) reported as uncertainty bounds. The maximum discharge was reconstructed for the four largest events and the highest event of the monitoring period, at 10–12 August 2015, with an estimated 50 yr return period. The latter return period is a rough estimate to provide some longer-term context based on the highest recorded rainfall amount and intensity since on-site meteorological measurements began in 2008. Further, the changes to the stream channel were not observed by long-term staff members since the establishment of the research station in 1976. Most importantly, riparian trees (higuerones, *Ficus spp.*) of 30 m height estimated by plant physiologists to exceed 100 years of age were removed by the extreme event. As evidenced by the consistency in gaugings in Fig. 4, the channel geometry itself did not change after this large event, so that the same rating curve is applied consistently in time. Uncertainty in the rating curve is highest for the high discharges due to a strong non-linearity induced by the extreme event that exceeds 100-fold the second largest event (Fig. 4 inlet). All data were directly used for analysis without gap filling in case of sensor failure.

Turbidity measurements were recorded in Nephlometric Turbidity Units (NTU). Continuous, at least monthly, maintenance and cleaning prevented sensor failure. In addition, there was little possibility for debris build-up around the optical sensor due to the high flow velocities (> 2 m/s) during events. Stream water samples (n = 23) were manually taken using a standard DH-48 sediment sampler across a range of level and turbidity conditions in an attempt to relate the mass of sediments to the NTU data. These stream water samples were processed to obtain the total of suspended and dissolved sediments (American Public Health Association, 1999). The spatial variability in sediments was assessed by collecting manual sediment samples in seven different tributaries on both hillslopes (A, B) and in the main stream (Fig. 3). To further determine the impact of main rainfall events, this was done before and after the 50 yr return period flood event. All samples were completely dried for 3 h at 105 °C, treated with H_2O_2 to remove organic material and then washed and dried again. The sediments were processed to obtain the particle size distribution curve using a set of 19 (Fisher Scientific) sieves varying from 8 to 0.05 mm and the Retsch As200 sieve shaker. The material remaining in each sieve was weighed and visualized as cumulative percentages. The 0.25 mm quartz diameter was selected for a morphoscopic analysis conducted using a Meiji PBH Stand stereoscope (Tricart, 1965). Landslides were mapped after the extreme event and the dimension documented with digital imagery. The landslide volumes were derived from a post-event interpretation of georeferenced photographs converted into 3D imagery using the *Agisoft Photoscan* software.

To assess stream sediment in the context of potential source areas, 26 soil samples (0 to 30 cm depth) were taken at accessible sites across the catchment (Fig. 3) and analysed for soil texture. Eighteen samples were processed using the pipette method (Veas, 2009) at an earlier time and eight samples using Bouyoucos method over the study period. Despite slight differences in the analytical protocol, both methods provided comparable results using duplicate measurements for comparison (Norambuena et al., 2002). The texture of the soils was determined using the USDA textural triangle (Henríquez and Cabalceta, 2012).

To monitor erosion and/or deposition of material on both hillslopes, at different altitudes and slopes, soil movement was assessed using a total of 10 erosion pins following Hancock and Lowry (2015). The pins consisted of 60 cm length steel rods with a > 0.6 cm diameter and were painted with anticorrosive yellow. They were inserted manually (site conditions allowing) without a hammer (Hancock and Lowry, 2015) as depth markers. Readings with an approximate error of 0.2 cm were done monthly by the same person during the rainy season and during the dry season the data were collected twice in January and once at the end of May after the rainy season 2016 started.

2.3. Statistical analysis

We analysed the rainfall-runoff-turbidity dynamics of the study site for a range of different events, which also included a major flood event during August 2015. The identification and definition of an event considered in this study was done systematically and based on both precipitation and discharge data. The start of precipitation indicates the beginning of an event, while the end of the discharge recession curve defined the end of the event. To be able to clearly identify event characteristics, we also imposed a threshold of a minimum water level change of 0.1 m. Double-peak runoff events were not detected.

Descriptive event statistics were used to explore 26 hydro-meteorological variables that characterize the size, range, minimum, maximum, mean, magnitude, intensity, duration of rise and recession and time lag of the precipitation-discharge-turbidity relationship of each selected event, as well as the antecedent wetness conditions for 3, 7 and 30 days plus the time (hours) without rainfall prior to an event. The hysteresis index of Zuecco et al. (2016) was applied using discharge as the independent variable and turbidity as the dependent variable. Among many other hysteresis indices available, the index by Zuecco et al. (2016) is a dimensionless number allowing for automatic and objective calculation of all the forms of possible hysteresis loops, sizes and directions found here. The selected events were further separated into dry (January to April) and wet (May to December) season and before and after the major event in August 2015 mainly due to the climatic seasonality of the study site and the impact caused by the event.

Spearman rank correlation (r) and Principal Components Analysis (PCA) were applied to reduce the number of environmental variables avoiding co-linearity as indicated by an r > 0.7 and to search for

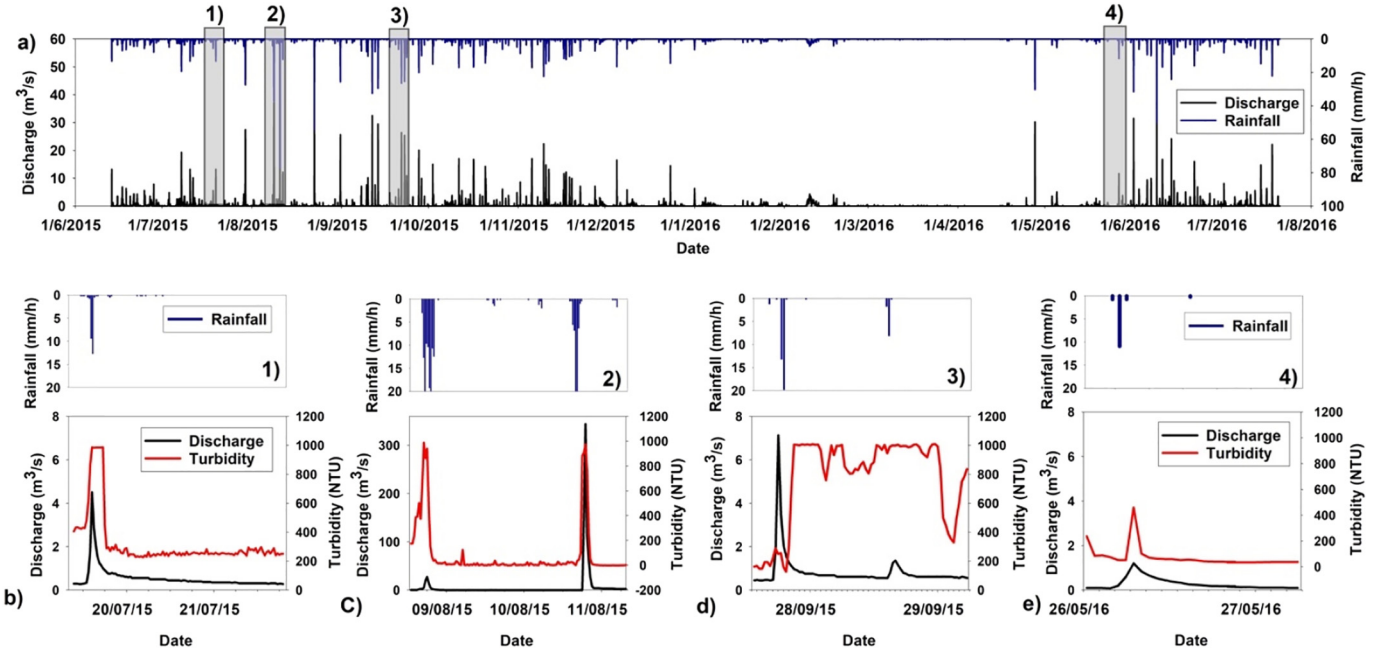

Fig. 5. a-b) Average hourly rainfall-runoff time series for the study period with four selected events marked with grey bars emphasizing the discharge-turbidity dynamics during 1) the rainy season before the extreme event, 2) the major event in August 2015, 3) post-event during the rainy season and 4) at the beginning of the rainy season in May 2016. All scales are comparable apart from the major event (2) occurred in August 2015 showing a different scale for visualization purposes.

relationships that could potentially explain the rainfall-runoff-turbidity dynamics of the study site (see Abbreviations of selected variables). Selected variables for correlation analysis were additionally checked for co-linearity using the Variance Inflation Factor. Cumulative particle size distributions and the shape and oxidation level of sediment samples were used to examine spatial variability across the main stem and tributaries before and after the major event in August 2015. A Kruskal-Wallis test was applied to the sediment data to determine the statistical evidence of significant changes associated to the rainy and dry season events, and the major flood event (R Core Team, 2016).

3. Results

3.1. Rainfall-runoff event and turbidity dynamics

The study year was characterized by a record El Niño event (NOAA, 2016) resulting in lower than average annual precipitation (~2700 mm/yr, Table I). Despite the generally drier conditions on the Pacific slope, the catchment locally received a record convective rainfall event in August 2015 resulting in a likely > 50 yr return period flood event. A total of 29 rainfall events were selected over the study year from 13/06/2015 to 13/06/2016 (Fig. 5, Table II). From the 26 hydro-meteorological variables, 8 (Table II, Abbreviations) were used to describe the temporal dynamics of events explaining 92% of the total variance based on three Principal Components. The other 18 variables mostly resuming initial and recession conditions of events were neglected due to $r > 0.7$ indicating co-linearity. Furthermore, the 8 selected parameters showed small effects of co-linearity tested using the Variance Inflation factor resulting in values smaller than 6 for all cases. Table II gives the full spectrum of events and analysed variables with the overall mean and standard deviation.

As the hydrometerological conditions, in particular rainfall, are distinctly different for different seasons (Fig. 1), we first describe the rainfall-runoff and turbidity event dynamics for each wet and dry season cycle based on the typical climatic features of the study site. Out of the total 29 events, 25 occurred during the 2015 rainy season from June to December. During this rainy season, the precipitation magnitude ranged from 2.8 to 132.3 mm, with average rainfall duration of 5.4 h. The turbidity increased up to a maximum value in almost half of the events. The median time lag between the rainfall peak and maximum discharge was 1 h. The median time lag between the discharge peak and the turbidity peak was also 1 h, while the median time between the peaks of precipitation and turbidity was 2.5 h (Fig. 5), but generally lags followed a normal distribution.

During the dry season 2016 (January–April) only two out of the 29 events were identified (Fig. 5), despite more sporadic rainfall originating from the Caribbean. The magnitude of the two precipitation events was 19.3 and 45.2 mm (for the first and second event, respectively). The discharge range reported was from 0.4 to 0.8 m^3/s and events lasted from 1.5 to 8.5 h, while the turbidity reached maximum values just once (Fig. 5).

Likewise, also only two events were identified for the beginning of the rainy season in May 2016. The magnitude *M* of these precipitation events was 12.7 mm and 35.6 mm (Table II). The discharge range reported was 1.1 m^3/s and 1.7 m^3/s respectively, while the turbidity reached relatively low values in both events (Fig. 5).

The runoff-turbidity data showed distinctly different hysteresis patterns for periods before the main August 2015 event and during the recovery period. The events before August 2015 did show few hysteresis patterns exhibiting a clockwise behaviour (Table II; Fig. 6, first panel). From August 2015, all events did indicate hysteresis patterns of discharge versus turbidity with changing clockwise and anti-clockwise loops (Fig. 6, second and third panel). The most frequent hysteresis class according to the classification of Zuecco et al. (2016) was class 2 (clockwise, increasing from initial values, but shape of an eight similar to event 3, second panel of Fig. 6). Apart from one class 6 and one class 5 event, no events that showed decreasing values from the initial state were detected (class 7 and 8). The hysteresis behaviour also shifted from no time lag to a relatively regular clockwise hysteresis including the major event in August (Fig. 5, event 2) to a more chaotic anti-clockwise and eight-shaped hysteresis pattern, back to initial conditions showing a clockwise hysteresis (Fig. 6, event 4).

Table II
The hydro-meteorological characteristics (8 variables) of the selected rainfall events during the study period (co-linear variables were removed) plus the hysteresis index of Zuecco et al. (2016) and classification are shown. The four events marked in italics were used for further analysis and note that the second (extreme) event marks the pre- and post-event periods used in the analysis. The mean and standard deviation was calculated without the August 2015 extreme event. The selected variables were a 7-day Antecedent Wetness Index – *AWI7d*, rainfall magnitude *M*, maximum rainfall intensity – *Imax*, discharge event range – *Q range*, lag time from rainfall peak to discharge peak – *P_Qlag*, turbidity event range – *Range*, lag time from rainfall peak to turbidity peak – *P_TUlag*, lag time from turbidity peak to discharge peak – *TU_Qlag*.

Event date	AWI7d (mm)	M (mm)	Imax (mm/h)	Q range (m^3/s)	P_Qlag (h)	Range (NTU)	P_TUlag (h)	TU_Qlag (h)	Hyst index	Hyst class
13–14/6/2015	74.89	13.21	13.21	0.34	1	587.66	6	6	0.063	2
16–18/6/2015	68.55	29.71	8.64	1.16	1	998.08	2.5	1.5	*	*
1) 19–20/6/2015	59.4	8.38	3.58	0.69	1.5	69.09	2.5	1	*	*
24–25/6/2015	58.87	22.05	7.36	0.79	7	413.01	8.5	1.5	*	*
26/6/−2/7/2015	75.84	26.63	3.55	1.26	13.5	463.3	13.5	0	0.036	2
7–8/7/2015	42.81	38.08	19.3	3.08	3.5	204.4	0.5	0.5	0.065	2
10–11/7/2015	91.26	28.95	18.54	0.75	1	84.24	3.5	2.5	*	*
14–15/7/2015	127.32	2.78	2.03	1.69	2	786.55	2.5	0.5	−0.576	4
19–21/7/2015	39.5	25.13	22.1	4.2	1	580.82	4	3	−0.098	4
29–30/7/2015	29.11	56.65	27.43	17.25	0.5	704.43	−3.5	−2	0.545	1
8–10/8/2015	24.53	132.33	40.13	4.99	2.5	813.05	2.5	0	0.341	1
2) 10–11/8/2015	158.64	98.57	77.22	343.77	0	974.06	1	1	0.126	1
31/8–1/9/2015	8.61	59.19	29.72	1.75	0.5	929.61	1.5	1	−0.124	3
11–12/9/2015	55.34	44.95	32.51	9.62	1	760.64	7.5	6.5	0.11	1
13–14/9/2015	106.89	38.1	29.47	3.89	1.5	636.58	0.5	−1	0.186	2
17–18/09/2015	93.93	10.16	9.66	1.4	1	762	2	1	−0.32	4
19–20/09/2015	56.82	4.32	4.07	1.34	0.5	854.2	3	2.5	−0.558	4
20–21/09/2015	22.03	10.92	6.61	0.8	1	425	2.5	1.5	0.039	2
21–22/09/2015	32.2	48.01	32.52	14.3	1	722.1	1	0	0.127	1
22–23/09/2015	80.96	35.05	25.4	3.73	0.5	939.1	4	3.5	0.205	2
3) 27–28/09/2015	126.67	34.79	33.02	6.68	0.5	877.4	7	6.5	0.036	1
12–13/10/2015	76.82	8.64	5.59	1.11	1	906.9	9.5	8.5	0.213	5
16–18/10/2015	76.61	49.77	26.67	10.7	1.5	327.5	0	−1.5	0.215	1
20–23/10/2015	90.59	50.3	21.59	7.03	7.5	636.8	1.5	−6	0.033	2
05–07/11/2015	28.39	35.56	19.56	4.33	0.5	508.2	0.5	0	0.086	2
31/12/2015–02/01/2016	8.59	19.29	4.83	0.76	2.5	997.2	4.5	2	−0.628	4
27/4/2016	6.59	45.22	40.39	0.47	1	57.9	6	5	0.32	6
4) 26–27/5/2016	9.33	12.69	11.68	1.12	1.5	222.42	1.5	0	0.064	2
31/5–2/6/2016	34.73	35.56	31.5	2.72	1	191.77	0.5	−1	−0.016	3
Mean:	*57.4*	*33.1*	*18.9*	*3.9*	*2.1*	*587.9*	*3.4*	*1.5*		
Std. dev.:	*35.0*	*25.4*	*12.1*	*4.4*	*2.8*	*298.6*	*3.5*	*3.0*		

* no hysteretic behaviour detected.

3.2. Impacts of an extreme event on the rainfall-runoff response and turbidity dynamics

During August 2015, two consecutive convective storms in < 36 h triggered an estimated 50 yr return period flood event. Antecedent rainfall was 24 mm over 7 days with relatively dry soils before the first storm. On the first day, 132 mm of precipitation fell in < 4 h with a maximum intensity of 40 mm in 30 min (Fig. 5, event 2). This storm caused water levels to rise 1.14 m with a discharge of around 25 m^3/s in < 3.5 h, with corresponding maximum turbidity levels of > 900 NTU.

The second event occurred 14 h after the previous storm, with soil saturation at a maximum, and an additional accumulated 147 mm of rain in 4 h. The maximum intensity was 77 mm in < 30 min resulting in a water level increase of up to 2.86 m. The reconstructed flood peak discharge based on flood marks using Manning's equation resulted in approximately 370 ± 56 m^3/s. Turbidity levels were beyond 1000 NTU. A total accumulated rainfall of 279 mm revealed (post-event field inspections) important morphological changes in the river network and over 15 landslides contributing an estimated > 100 m^3 of material were identified along the stream. Tributaries were also intensively modified by incorporation of rocks, sediments, and vegetation from the slopes

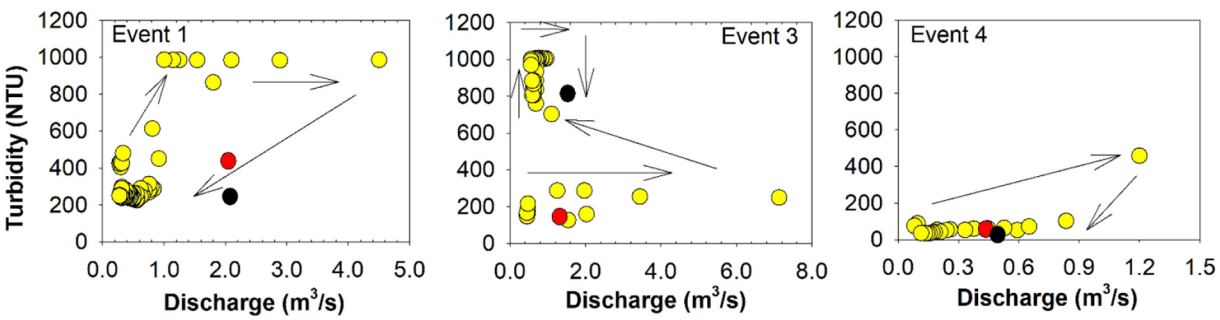

Fig. 6. Discharge – turbidity hysteresis plots for pre-flood event (event 1 in Fig. 4) conditions (clockwise hysteresis), post-flood event (event 3 – anti-clockwise and eight-shaped hysteresis) and recovery conditions (event 4 – clockwise hysteresis). The turbidity scale is comparable for visualization purposes and the numbering of events corresponds to Fig. 4. Red dots mark the starting discharge and turbidity, black dots indicate the end of the event and the arrows give the hysteresis direction. (For interpretation of the references to colour in this figure legend, the reader is referred to the web version of this article.)

Table III
Pre-event (upper panel in Grey italics) and post-event (lower panel in black) Spearman rank correlation matrix of eight selected rainfall-runoff-turbidity parameters. Statistical significance is given by asterisks (* = 90%, ** = 95% and *** = 99%).

	AWI7d (mm)	M (mm)	Imax (mm/h)	Qrange (m^3/s)	P_Qlag (h)	Range (NTU)	P_TUlag (h)	TU_Qlag (h)
AWI7d (mm)	1	*−0.61 (*)*	*−0.84 (**)*	*−0.66 (*)*	*0.13*	*−0.19*	*0.34*	*0.27*
M (mm)	**−0.01**	1	*0.81 (**)*	*0.58 (*)*	*−0.19*	*0.33*	*−0.46*	*−0.42*
Imax (mm/h)	**0.1**	**0.71 (**)**	1	*0.65 (*)*	*−0.41*	*0.22*	*−0.4*	*−0.1*
Qrange (m^3/s)	**0.47**	**0.63 (**)**	**0.48**	1	*−0.17*	*0.58 (*)*	*−0.42*	*−0.52*
P_Qlag (h)	**−0.13**	**0.36**	**−0.1**	**−0.03**	1	*−0.19*	*0.44*	*−0.24*
Range (NTU)	**0.4**	**−0.42**	**−0.38**	**0.01**	**−0.23**	1	*−0.19*	*−0.27*
P_TUlag (h)	**−0.01**	**−0.4**	**−0.07**	**−0.4**	**−0.28**	**0.56 (*)**	1	*0.45*
TU_Qlag (h)	**−0.04**	**−0.48**	**−0.03**	**−0.38**	**−0.54 (*)**	**0.52 (*)**	**0.93 (***)**	1

(Fig. 2E).

At the catchment level, the extreme flood event from August 2015 had some remarkable consequences in terms of erosion and material transport (Fig. 2A). The turbidity response to rain events became slightly faster by around 30 min and reached maximum levels around 1000 NTU with less precipitation after the flood event (Table II). The stream reached maximum turbidity levels with on average lower precipitation inputs and rain intensity (Fig. 5, event 3; Table II). A Spearman rank correlation matrix was used to show differences in the time lag between the peaks of precipitation, discharge and turbidity before and after the extreme event (Table III). The rainfall-runoff dynamics before the extreme event were mostly related to antecedent conditions with a significant correlation ($p < 0.1$) of *AWI7* to discharge range (*Qrange*) of $r = -0.66$ and rainfall intensity *Imax* to *Qrange* with $r = 0.65$. No significant correlations to lag times were detected prior to the extreme event. The rainfall magnitude *M* and *Imax* were only moderately correlated to the rainfall-runoff lag *P_Qlag* ($r = -0.45$) and the *P_NTUlag* with $r = -0.42$. The discharge range was only moderately correlated to the turbidity range (*NTUrange*) ($r = 0.58$).

After the extreme flood event, the antecedent conditions played no role on rainfall-runoff and turbidity dynamics (Fig. 7b). However, the rainfall magnitude *M* was significantly correlated to discharge ($r = 0.63$, $p < 0.05$), and correlated to *P_Qlag* ($r = 0.36$) and rainfall and discharge, turbidity lag time ($r = -0.4$ and -0.48, respectively). The *P_Qlag* was also significantly related to *Q_NTUlag* with $r = -0.54$ ($p < 0.1$) meaning the longer the rainfall-runoff response time is the shorter the runoff-turbidity response. After the event, the *NTUrange* was significantly correlated to rainfall-turbidity lag time ($r = 0.56$, $p < 0.1$) and discharge-turbidity lag time (0.52, $p < 0.1$). A Kruskal-Wallis test was applied to the 8 selected variables before and after the event. The results of significance values p varied from 0.02 to 0.75 with the lag time of discharge to turbidity resulting in the only significant change at the 95% level.

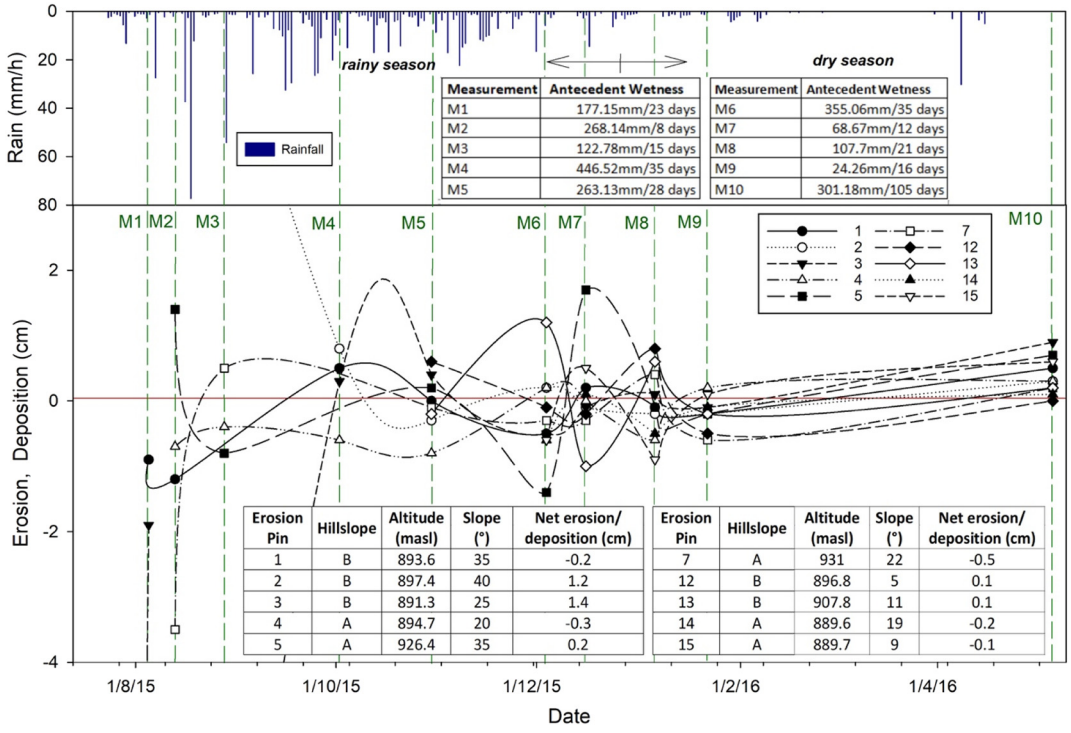

Fig. 7. Soil movement was detected using erosion pins for the study period 2015–16 with the sites (see Fig. 2) main physical characteristics (slope and altitude) and the accumulated rainfall between measurements. Negative values represent erosion and positive values represent deposition (accumulation of material). The measurements were connected with smoothed lines to emphasize the temporal variability over the roughly monthly interval. Erosion pin 3 showed the largest soil erosion and pin 2 the largest deposition (both on hillslope B).

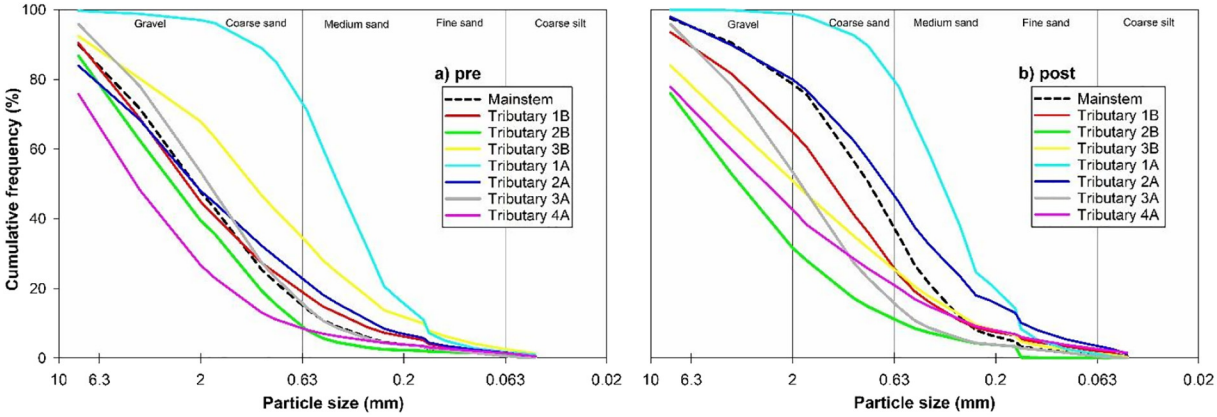

Fig. 8. The figure shows the particle size distributions of stream sediments sampled a) before and b) after the major flood event across the drainage network and tributaries as indicated in Fig. 2 (A, B corresponds to the hillslope location and the increasing numbering of upstream tributaries).

3.3. Sediment sources and connectivity

3.3.1. Soil erosion measurements

Data recordings at the erosion pins showed that erosion was most prominently detected after the major event in August 2015 with a maximum soil loss and deposits of over 10 cm at various sites. However, the movement of materials in terms of erosion and deposition was variable across all sites. Fig. 8 indicates that most material was mobilised towards the end of the rainy season (Fig. 8 – M6, M7) with more accumulated rainfall. The erosion pins also showed that all sites were characterized by gaining and losing conditions at some point across variable 9 to 35 degrees steep slopes. Net erosion and net deposition was equally recorded at 5 sites each after the complete 1-year study period.

Fig. 8 shows particle size distributions sampled from 1 week before and immediately 3 days after the extreme event for the main stem and three to four tributary streams on both hillslopes A and B (see Fig. 3, sampling sites). The data for the main stem show that after the event, the dominant particle size was generally smaller (mainly medium to course sand), than prior to the event (mainly coarse sand to gravel). Most tributaries (1A, 2A, 2B and 4B) showed a similar shift in behaviour after the event. In contrast, the tributaries 3A and 4A accumulated coarser grained material after the event, while the particle size distributions of tributaries 1B and 3B remained largely the same. The granulometric curves identified mainly coarse particle sizes and only < 5% of all sediment samples collected were composed of silt. The latter material properties might also be related to a slightly different tributary catchment morphology with more moderate slopes (Fig. 3) and finer material on hillslope A as opposed to coarser material on hillslope B.

3.3.2. Turbidity as an indicator of sediment loads

Even though we focussed primarily on the temporal dynamics and potential processes that affect the rainfall-runoff-turbidity behaviour, we also explored the use of turbidity as an indicator for suspended sediment flux. Sediment particle size analyses from the 23 sampled storm events indicated that all sand and coarser material in the samples corresponded with turbidity measurements < 200 NTU (Fig. 9). Maximum turbidity exceeding 1000 NTU appeared to be generated by finer dissolved particles (fine sands and silt). In absence of a significant amount of superficially available clay particles (Fig. 3c), the silt fraction was therefore responsible for most of the turbidity generated (Fig. 9). The sand fraction did not result in turbidity higher than 50 NTU. However, silty material was < 5% of the stream sediment composition (pre- and post-event) and < 30% of hillslope soils in the catchment. Even small amounts of silt caused high turbidity independently of the total transported and sampled mass (Fig. 9B). No relationship between turbidity, suspended sediment concentration SSC (g/L) and discharge was hence detected for construction of a reasonable rating curve during the study period (Fig. 9A).

4. Discussion

4.1. Characterizing rainfall-runoff-turbidity dynamics in tropical, volcanic catchments

Among the first from humid tropical volcanic regions, our results showed that rainfall-runoff-turbidity dynamics in the San Lorencito catchment are driven by hydroclimatic conditions and can be further linked to heterogeneity in catchment characteristics and material properties of soils, and bedrock. The climatic seasonality exhibited a high inter-event variability of the rainfall-runoff-turbidity relationship particularly during the rainy season (Table II). The values of turbidity were generally higher during the months from May to December (Table II). The runoff generation in this steep and tropical setting causes - as can be expected (see Zimmermann et al., 2012) – a quick runoff response to rainfall inputs in the order of 30 to 40 min. However, there is an important surface runoff generation component (Dehaspe et al., 2018) contrary to other studies from similar systems that reported mostly sub-surface storm runoff generation (Muñoz-Villers and McDonnell, 2012). The rainfall-runoff response was unsurprisingly characterized by a significant relationship with the antecedent wetness and storm characteristics such as rainfall intensity, while we detected no significant rainfall-runoff-turbidity lags (Table III). However, the drivers of the rainfall-runoff response were less dominated by the wetness state of the catchment and rainfall intensity immediately after the impact of an extreme event that significantly modified the fluvial geomorphology of the catchment. In addition, there were significant lag times in the turbidity response to rainfall and discharge during that time. As such, we found complex discharge – turbidity hysteresis characteristics that shifted in shape and magnitude after the extreme event (Table III – Fig. 6). It is likely that this can be explained by shifts in the sediment sources, which in turn result in variations in the material itself (e.g. particle size, as shown by Cheraghi et al. (2016)), but also the transport and delivery characteristics. Some events at the beginning of the rainy season 2015 and before the extreme event did not show hysteresis, and others were characterized by more complex temporal relationships (35%). We observed mostly eight-shaped hysteretic patterns (49%) after the major flood event, while only 3% of events showed positive (clockwise) hysteresis in contrast to López-Tarazón and Estrany (2017) from a Mediterranean catchment and 13% showed negative (counter clockwise) hysteresis. Eight-shaped hysteresis loops have previously been classified as less common and difficult to decipher in geomorphologically different study areas (e.g. Hudson, 2003; Perks

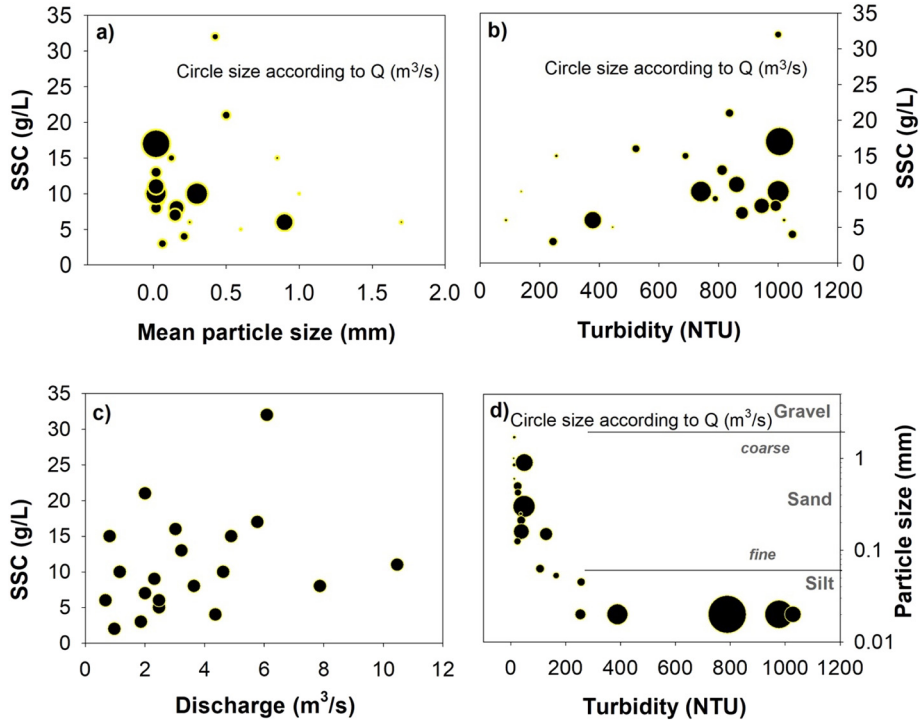

Fig. 9. a) the mean particle size – suspended sediment concentration (SSC in g/L) – discharge (Q) visualization from 0.2 to 10 m^3/s is plotted for 23 storm event samples and b) the SSC and turbidity level.

et al., 2015).

4.2. The role of extreme events on sediment transport dynamics and fluvial geomorphology

The transformation of fluvial systems mostly happens during extreme events, when equilibrium river channel parameters and slope gradients may be disturbed and the thresholds controlling fluvial or gravitational processes may be exceeded (Thomas, 1994). Among the hydro-meteorological extreme events are those characterized by low exceedance probabilities of precipitation and runoff. Even though our exceedance probability estimate of 50 years for the August 2015 extreme event is rather uncertain, the empirical evidence suggested an extreme event previously not observed for over 30 years. The orographic ascend of Caribbean trade winds maintain a constant humidity most of the year with intense convective rainstorms originating from the Pacific Ocean that caused the observed extreme runoff response and was the most intense rainfall event of such a magnitude since measurements from 2008. The combination of both precipitation mechanisms - a constant low intensity input of rainfall and intense convective storms - causes saturation excess overland flow with possibly associated laminar erosion (in contrast to sub-surface stormflow generation on volcanic substrate identified by Muñoz-Villers and McDonnell, 2012 in Mexico). Material movement on the hillslopes was clearly detected by the erosion pins (Fig. 8) particularly during the extreme event with soil losses and deposits of up to 10 cm.

Furthermore, the San Lorencito stream is controlled by a system of parallel normal faults with SW-NE orientation; the direction in which the main channel drains (see Fig. 1b, Denyer et al., 2003). Tectonic joints on the volcanic rocks can be observed along the stream channel outcrops, which is a pre-condition for exposed material and subsequent potential rapid incorporation into the stream in extreme conditions. The extreme event described above created alluvial deposits (in parts areas > 1800 m^2) along the riparian zone and removed riparian vegetation (Fig. 2A). In addition, tributaries built up alluvial fans among deepening and widening of channels that caused the stream to abandon a certain stream section (Fig. 2E). The flood debris flow deposited large amounts of material on abandoned fluvial terraces, and in other cases large deposits of young fluvial terraces where eroded (Fig. 2F). The latter type of material close to the main channel can be incorporated and transported in short periods of time. Large rounded boulders such as in Fig. 2F evidenced the torrential behaviour and stream capacity of recent and historic extreme events. Therefore, the study catchment can be characterized by an easy mobilization of colluvial (mainly landslides and laminar soil erosion) and alluvial material (stream bank and terrace erosion). Nevertheless, such extreme events are part of the normal denudation on geological scales as suggested by deep scars of mass movement on the hillslopes (evidence from the elevation model in Fig. 1) and large fluvial terraces (in parts with ~20 cm of pedogenesis in Fig. 2F) strongly support recent Holocene torrential behaviour (Vargas, 1978).

4.3. Sediment sources and hillslope-stream connectivity

The periodic monitoring during sampling campaigns showed that the tributaries influence the direction of streamflow and streambed incision (Fig. 2E). The high rainfall in excess of 40 mm/h in combination with variable geomorphological features of slope (e.g. on average lower slope on hillslope A compared to B) and soils (Fig. 3) and the vegetation density (Dehaspe et al., 2018) dictated that the spatial variability of the catchment's connectivity was high (Fryers, 2013).

We also identified around 15 landslides that directly contributed colluvial material (> 100 m^3) into the stream (Fig. 2G and location in Fig. 3). All rocks from the landslides were identified as jointed andesites with different levels of profile weathering. After the stream lost transport capacity during recession, the young incorporated material was deposited and readily available during subsequent minor events causing high levels of turbidity for a prolonged time after peak flow (see, e.g. Fig. 5 - event 3). All the landslides identified during this study (Fig. 3) occurred during the rainy season. They also contributed an important amount of hillslope material into the stream as part of or in addition to what was demonstrated by the monitored erosion pins (Fig. 8).

Further evidence of hillslope-stream connectivity was found in identical levels of mineral oxidation of sandy sediments recovered from soil, tributary and main stem sediment samples (Fig. S1). Seasonal patterns in sediment delivery, transport and deposition from the rainy season into the dry season have been previously related to the rainfall regime with an increase in rainfall events leading to an increased sediment yield (Thomas, 1994; Fryers, 2013). This is in agreement with our results, even though we were limited by only using soil erosion measurements and turbidity as an indicator for temporal dynamics in suspended sediments. Nevertheless, the transit of material from the hillslopes to the stream and within the channel appeared to occur throughout the year, even though the frequency of rainfall events was less during the dry season. Such high rainfall probability despite a climatic seasonality occurred similarly in other catchments on the south Pacific slope (Birkel et al., 2016). During the dry season, drying soils allowed for relatively more water to infiltrate (Fig. 5b – dry season rainfall events did result in very minor runoff response), limiting the means for particles to erode from the hillslopes (Fig. 8). The relatively slow and limited sediment movement during the dry season was therefore dominated by readily available material stored in the channel or from channel erosion since the channel sediments were mostly sands with < 5% fine sandy aggregates (Fig. 7) and these particles have a higher settling velocity than the silts and clays originating from the hillslopes. Much of the hillslope sediment movement with erosion and deposition was generated during the rainy season (Fig. 8).

Sediment monitoring revealed two main types of sediment sources to the stream: Firstly, hillslope material that was fed into the stream and tributaries through landslides, colluvial, and surface erosion (similar to agricultural sites in the tropics, Duvert et al., 2010). Secondly, material deposits that formed fluvial terraces and sediment banks in areas of low stream power. The sediment particle distributions of the main stem and tributaries revealed that these were mostly coarse sand and gravel particles (~95%). The fine sand and coarse silt particles represented < 5% of all sediment samples (see Fig. 9). Sediments also exhibited an intense oxidation and weathering of minerals (composed primarily by Phenocrystals such as plagioclase, augite, magnetite, hornblende, quartz, olivine, biotite) similar to the dominating sand-silt soil samples as shown in Fig. 3 and Fig. S1. Similarities found in terms of morphology, particle size distribution, mineralogy and oxidation of sands provided evidence of a hillslope – stream connection mainly due to erosion caused by periodic surface runoff generation under more extreme rainfall (Fig. 5). The most likely mechanism was saturation excess overland flow (Dehaspe et al., 2018), since soils throughout the catchment have high infiltration capacities in excess of 200 mm/h (in contrast to Zimmermann et al., 2012). Under such extreme conditions, the dense forest cover does not play a significant role on flood generating runoff mechanisms anymore (e.g. Birkel et al., 2012 from another tropical volcanic Costa Rican catchment) that can also be associated to dominate material transport in steep, tropical, volcanic catchments.

Contrary to other extra-tropical studies (e.g. Hudson, 2003; Rovira and Batalla, 2006), we excluded a sediment exhaustion effect over the year. In the San Lorencito catchment, sediments seemed to always be available and constantly moving, even though there was sediment depletion over the dry season due to less rainfall events, increased infiltration of soils and the interception effect of the vegetation cover on the hillslopes. It might well be that sediment availability is key for rapid landscape transformations in the humid, volcanic tropics. However, more measurements combining sediment fingerprinting similar to Duvert et al. (2010) and Martínez-Mena et al. (1999) with efforts to quantify loads and their particle size distribution over a longer period will be necessary to confirm these initial results.

5. Conclusions and outlook

The challenge of working in tropical environments is partly reflected in less monitored catchments on a global scale. For example, the recent global review on erosion and sediment dynamics in the tropics by Labrière et al. (2015) did not include any study from Central America as an indication of the under-represented monitoring in the region. Apart from the study by Jansson (2002) that looked at event-scale SSC – Q hysteresis to determine sediment sources and the large-scale study by Krishnaswamy et al. (2001a, 2001b), there are to the best of our knowledge no systematic high-temporal resolution studies reported in the literature. Ziegler et al. (2014) estimated the uncertainty in SSC – Turbidity data from Thailand to be a major source of error in high load estimates over longer periods. In that sense, sensor equipment with a large NTU range (0 to 10,000 NTU) is needed to capture the complete variability of runoff – turbidity events. Such events need to be accompanied by high-resolution sediment sampling with an appropriate sampling strategy that captures the complete particle size classes from fine to coarse material.

The hillslope – stream connectivity can only quantitatively be assessed with automatic measurements of eroded material volumes and particles from the hillslopes at the same (or close) temporal sampling resolution. Our soil erosion measurements adapted from Hancock and Lowry (2015) in combination with a morphometric analysis of soils and sediments provided some evidence of such a hillslope – stream connectivity. However, estimates of erosion rates will need either a process-based model analysis using our preliminary data or a sediment fingerprinting in form of e.g. radioisotope analysis and/or a combination of both to further explore and quantify sediment loads and landforming processes.

This study aimed to gain more insights into the spatio-temporal variability of sediment sources, availability, and transport dynamics in humid tropical volcanic landscapes via intense monitoring. The study emphasized the importance of combined hydro-geomorphic data collection using high temporal resolution sensors and basic synoptic surveys of soil erosion and sediment material properties. In summary, our results indicated that sediment transport dynamics in steep humid tropical volcanic areas, as represented by the study catchment, are highly dynamic by nature against a background of high but unquantified sediment loads. Generally, sediments were supplied to the stream from the hillslopes in the form of laminar erosion triggered by saturation excess overland flow. However, extreme events with the occurrence of landslides exert an overriding impact on sediment dynamics even with 100% primary rainforest cover. In response to such an extreme event, runoff-turbidity relationships switched from a non-hysteretic to a strongly hysteretic behaviour after the extreme event. Nevertheless, our results indicated that the system of sediment dynamics was very resilient, as the post-event recovery was relatively quick (around 3 months). We also found that during our preliminary monitoring in the tropical, tertiary volcanic environment of the study site, turbidity and discharge are only weak indicators of sediment load and no meaningful discharge – SSC rating curve could be developed (Fig. 9). This might limit the use of turbidity data for use of sediment load studies in these environments, but we need more data over much longer measurement periods to be affirmative.

We conclude that more studies are needed in tropical, volcanic catchments to provide high-resolution baseline data for process-based model development applied to inform water users such as e.g. hydropower companies about the natural sediment load dynamics and budgets of headwater catchments that provide much of the ecosystem services used downstream. This study provided important first insights into the timing of sediment dynamics and allowed for the formulation of preliminary hypotheses of sediment sources and transport mechanisms. However, to quantify these aspects of hillslope-stream connectivity, we need to combine high temporal resolution monitoring over longer time periods with high spatial resolution erosion and sediment measurements. Remotely sensed imagery from LiDAR-equipped drone applications and radioisotopes for sediment fingerprinting might help in this regard and allow us to quantitatively assess

geomorphological changes to stream networks and their transport rates in tropical, volcanic catchments.

Supplementary data to this article can be found online at https://doi.org/10.1016/j.catena.2019.104118.

Acknowledgements

A British Geomorphological Society early career grant to JG and CB allowed initiating this work. An Ideawild grant to CB contributed with an equipment donation. The University of Costa Rica Research Council (projects B4239, B8709) supported this project. We thank the ReBAMB staff and students for helping with logistics and fieldwork. CIGEFI at UCR contributed with meteorological data. The data can be obtained upon request from the corresponding author.

References

American Public Health Association, American Water Works Association, Water Environment Federation, 1999. Standard Methods for the Examination of Water and Wastewater. (United States).

Bergoeing, J.P., 2007. Geomorphology of Costa Rica. Librería Francesa: San José, Costa Rica.

Birkel, C., Soulsby, C., Tetzlaff, D., 2012. Modelling the impacts of land cover change on streamflow dynamics of a tropical rainforest headwater catchment. Hydrol. Sci. J. https://doi.org/10.1080/02626667.2012.728707.

Birkel, C., Geris, J., Molina, M.J., Mendez, C., Arce, R., Dick, J., Tetzlaff, D., Soulsby, C., 2016. Hydroclimatic controls on non-stationary stream water ages in humid tropical catchments. J. Hydrol. 542, 231–240. https://doi.org/10.1016/j.jhydrol.2016.09.006.

Bonell, M., Bruijnzeel, L.A., 2005. Forests, Water and People in the Humid Tropics. Cambridge University Press, Cambridge. https://doi.org/10.1017/CBO9780511535666.020.

Bracken, L.J., Wainwright, J., Ali, G.A., Tetzlaff, D., Smith, M.W., Reaney, S.M., Roy, A.G., 2013. Concepts of hydrological connectivity: research approaches, pathways and future agendas. Earth Sci. Rev. 119, 17–34. https://doi.org/10.1016/j.earscirev.2013.02.001.

Buendia, C., Vericat, V., Batalla, R.J., Gibbins, C.N., 2015. Temporal dynamics of sediment transport and transient in-channel storage in a highly erodible catchment. Land Degrad. Dev. 27, 1045–1063. https://doi.org/10.1002/ldr.2348.

Calvo, J., 1998. Suspended sediment yield prediction models for Costa Rican watersheds. International Association of Hydrological Sciences. 253, 27–32.

Chang, J.H., Lau, L.S., 1983. Definition of the humid tropics. In: Humid Tropics, Bonell M., Hufschmidt, M.M., Gladwell, J.S. (Eds.), Hydrology and Water Management in the. Cambridge University Press, Cambridge, pp. 571–575.

Chappell, N.A., Douglas, I., Hanapi, J.M., Tych, W., 2004. Sources of suspended sediment within a tropical catchment recovering from selective logging. Hydrol. Process. 18, 685–701. https://doi.org/10.1002/hyp.1263.

Cheraghi, M., Jomaa, S., Sander, G.C., Barry, D.A., 2016. Hysteretic sediment fluxes in rainfall-driven soil erosion: particle size effects. Water Resour. Res. 52, 8613–8629. https://doi.org/10.1002/2016WR019314.

Chow, V.T., 1959. Open Channel Hydraulics. McGraw-Hill, New York.

Dehaspe, J., Birkel, C., Tetzlaff, D., Sánchez-Murillo, R., Durán-Quesada, A.M., Soulsby, C., 2018. Spatially distributed tracer-aided modelling to explore water and isotope transport, storage and mixing in a pristine, humid tropical catchment. Hydrol. Process. 32, 3206–3224. https://doi.org/10.1002/hyp.13258.

Denyer, P., Montero, W., Alvarado, G.E., 2003. Atlas tectónico de Costa Rica. In: UCR: San José.

Downing, J.A., Cole, J.J., Duarte, C.M., Middelburg, J.J., Melack, J.M., Prairie, Y.T., Kortelainen, P., Striegl, R.G., McDowell, W.H., Tranvik, L.J., 2012. Global abundance and size distribution of streams and rivers. Inland Waters 2, 229–236. https://doi.org/10.5268/IW-2.4.502.

Duvert, C., Gratiot, N., Evrard, O., Navratil, O., Némery, J., Prat, C., Esteves, M., 2010. Drivers of erosion and suspended sediment transport in three headwater catchments of the Mexican central highlands. Geomorphology 123, 243–256. https://doi.org/10.1016/j.geomorph.2010.07.016.

Fagan, M.E., DeFries, R.S., Sesnie, S.E., Arroyo, J.P., Walker, W., Soto, C., Chazdon, R.L., Sanchun, A., 2013. Land cover dynamics following a deforestation ban in northern Costa Rica. Environ. Res. Lett. 8. https://doi.org/10.1088/1748-9326/8/3/034017.

Foley, J.A., DeFries, R., Asner, G.P., Barford, C., Bonan, G., Carpenter, S.R., Chapin, F.S., Coe, M.T., Daily, G.C., Gibbs, H.K., Helkowsky, J.H., Holloway, T., Howard, E.A., Kucharik, C.J., Monfreda, C., Patz, J.A., Prentice, C., Ramankutty, N., Snyder, P.K., 2005. Global consequences of land use. Science 309. https://doi.org/10.1126/science.1111772.

Fryers, K., 2013. (dis)connectivity in catchment sediment cascades: a fresh look at the sediment delivery problem. Earth Surf. Process. Landf. 38, 30–46. https://doi.org/10.1002/esp.3242.

Giorgi, F., 2006. Climate change hot-spots. Geophys. Res. Lett. 33. https://doi.org/10.1029/2006GL025734.

González, J.E., Georgescu, M., Lemos, M.C., Hosannah, N., Niyogi, D., 2017. Climate change's pulse is in Central America and the Caribbean. Eos 98. https://doi.org/10.1029/2017EO071975.

Hancock, G.R., Lowry, J.B.C., 2015. Hillslope erosion measurement –a simple approach to a complex process. Hydrol. Process. 29, 4809–4816. https://doi.org/10.1002/hyp.10608.

Henríquez, C., Cabalceta, G., 2012. Guía práctica para el estudio introductorio de los suelos con un enfoque agrícola. Costa Rican Association of Soil Science: San José.

Hudson, P.F., 2003. Event sequence and sediment exhaustion in the lower Panuco Basin, Mexico. Catena 52, 57–76. https://doi.org/10.1016/S0341-8162(02)00145-5.

Jansson, M., 2002. Determining sediment source areas in a tropical river basin, Costa Rica. Catena. 47, 63–84.

Krishnaswamy, J., Halpin, P.N., Richter, D.D., 2001a. Dynamics of sediment discharge in relation to land-use and hydro-climatology in a humid tropical watershed in Costa Rica. J. Hydrol. 253, 91–109. https://doi.org/10.1016/S0022-1694(01)00474-7.

Krishnaswamy, J., Richter, D., Halpin, P., Hofmockel, M., 2001b. Spatial patterns of suspended sediment yields in a humid tropical watershed in Costa Rica. Hydrol. Process. 5, 2237–2257. https://doi.org/10.1002/hyp.230.

Labrière, N., Locatelli, B., Laumonier, Y., Freycon, V., Bernoux, M., 2015. Soil erosion in the humid tropics: a systematic quantitative review. Agric. Ecosyst. Environ. 203, 127–139. https://doi.org/10.1016/j.agee.2015.01.027.

Loescher, H.W., Powers, J.S., Oberbauer, S.F., 2002. Spatial variation of throughfall volume in an old-growth tropical wet forest, Costa Rica. J. Trop. Ecol. 18, 397–407. https://doi.org/10.1017/S0266467402002274.

López-Tarazón, J.A., Estrany, J., 2017. Exploring suspended sediment delivery dynamics of two Mediterranean nested catchments. Hydrol. Process. 31, 698–715. https://doi.org/10.1002/hyp.11069.

Martínez-Mena, M., Alvarez-Rogel, J., Albaladejo, J., Castillo, V., 1999. Influence of vegetal cover on sediment particle size distribution in natural rainfall conditions, in a semiarid environment. Catena 38, 175–190.

Mills, C.F., Bathurst, J.C., 2015. Spatial variability of suspended sediment yield in a gravel-bed river across four orders of magnitude of catchment area. Catena. 133, 14–24. https://doi.org/10.1016/j.catena.2015.04.008.

Muñoz-Villers, L.E., McDonnell, J.J., 2012. Runoff generation in a steep, tropical montane cloud forest catchment on permeable volcanic substrate. Water Resour. Res. 48. https://doi.org/10.1029/2011WR011316.

NOAA, 2016. http://www.cpc.ncep.noaa.gov/products/analysis_monitoring/ensostuff/ensoyears.shtml last visited July 2017.

Norambuena, P., Luzio, W., Vera, W., 2002. Comparison between the pipette and bouyoucos methods and their relation with water retention in eight soils of the andean plateau, Parinacota Province, Chile. Agricultura Técnica. 62. https://doi.org/10.4067/S0365-28072002000100015.

Perks, M.T., Owen, G.J., Benskin, C.M., Jonczyk, J., Deasy, C., Burke, S., Reaney, S.M., Haygarth, P.M., 2015. Dominant mechanisms for the delivery of fine sediment and phosphorus to fluvial networks draining grassland dominated headwater catchments. Sci. Total Environ. 523, 178–190. https://doi.org/10.1016/j.scitotenv.2015.03.008.

R Core Team, 2016. R: A language and environment for statistical computing. R Foundation for Statistical Computing, Vienna, Austria. http://www.R-project.org/.

Rovira, A., Batalla, R.J., 2006. Temporal distribution of suspended sediment transport in a Mediterranean basin: the lower Tordera (NE Spain). Geomorphology. 79, 58–71. https://doi.org/10.1016/j.geomorph.2005.09.016.

Salazar-Rodríguez, A.H., 2003. Reserva Biológica Alberto Manuel Brenes: Una excepción en Costa Rica. Revista InterSedes 8.

Shanley, J.B., McDowell, W.H., Stallard, R.F., 2011. Long-term patterns and short-term dynamics of stream solutes and suspended sediment in a rapidly weathering tropical watershed. Water Resour. Res. 47. https://doi.org/10.1029/2010WR009788.

Sharon, D., 1980. The distribution of hydrologically effective rainfall incident on sloping ground. J. Hydrol. 46, 165–188. https://doi.org/10.1016/0022-1694(80)90041-4.

Thomas, M.F., 1994. Geomorphology in the Tropics: A Study of Weathering and Denudation in Low Latitudes. John Wiley and Sons, Chichester.

Tricart, J., 1965. Principes et méthodes de la géomorphologie. Masson et Cie Éditeurs, Paris.

Vargas, G., 1978. Diagnóstico y recomendaciones para el manejo y ordenamiento de los recursos naturales de la cuenca del río San Lorenzo, Alajuela, Costa Rica (unpublished thesis). University of Costa Rica.

Veas, N., 2009. Caracterización y estimación de la erosión laminar en un bosque premontano a partir de un modelado hidrológico. Microcuenca del río San Lorencito, Cordillera Volcánica de Tilarán, Costa Rica. (unpublished thesis). University of Costa Rica.

Walsh, R.P.D., Bidin, K., Blake, W.H., Chappell, N.A., Clarke, M.A., Douglas, I., Ghazali, R., Sayer, A.M., Suhaimi, J., Tych, W., Annammala, K.V., 2011. Long-term responses of rainforest erosional systems at different spatial scales to selective logging and climatic change. Philos. Trans. R. Soc. Lond. B 366 (1582), 3340–3353. https://doi.org/10.1098/rstb.2011.0054.

Wohl, E., Barros, A., Brunsell, N., Chappell, N., Coe, M., Giambelluca, T., Goldsmith, S., Harmon, R., Hendrickx, J., Juvik, J., McDonnell, J., Ogden, F., 2012. The hydrology of the humid tropics. Nat. Clim. Chang. 2, 655–662. https://doi.org/10.1038/nclimate1556.

Zhang, Z., Tao, F., Shi, P., Xu, W., Sun, Y., Fukushima, T., Onda, Y., 2010. Characterizing the flush of stream chemical runoff from forested watersheds. Hydrol. Process. 24 (20), 2960–2970. https://doi.org/10.1002/hyp.7717.

Ziegler, S.G. Benner, Tantasirin, C., Wood, S.H., Sutherland, R.A., Sidle, R.C., Jachowski, N.R.A., Lu, X., Snidvongs, A., Giambelluca, T.W., Fox, J.M., 2014. Turbidity-based sediment monitoring in northern Thailand: hysteresis, variability, and uncertainty. J. Hydrol. https://doi.org/10.1016/j.jhydrol.2014.09.010.

Zimmermann, A., Francke, T., Elsenbeer, H., 2012. Forests and erosion: insights from a study of suspended-sediment dynamics in an overland flow-prone rainforest catchment. J. Hydrol. 27, 170–181. https://doi.org/10.1016/j.jhydrol.2012.01.039.

Zuecco, G., Penna, D., Borga, M., van Meerveld, H.J., 2016. A versatile index to characterize hysteresis between hydrological variables at the runoff event timescale. Hydrol. Process. 30, 1449–1466. https://doi.org/10.1002/hyp.10681.